IMMUNOLOGY

Dissecting the role of CAR signaling architectures on T cell activation and persistence using pooled screens and single-cell sequencing

Rocío Castellanos-Rueda[1,2]*, Kai-Ling K. Wang[1], Juliette L. Forster[1], Alice Driessen[1,3], Jessica A. Frank[1], María Rodríguez Martínez[3], Sai T. Reddy[1]*

Chimeric antigen receptor (CAR) T cells offer a promising cancer treatment, yet challenges such as limited T cell persistence hinder efficacy. Given its critical role in modulating T cell responses, it is crucial to understand how the CAR signaling architecture influences T cell function. Here, we designed a combinatorial CAR signaling domain library and performed repeated antigen stimulation assays, pooled screens, and single-cell sequencing to systematically investigate the impact of modifying CAR signaling domains on T cell activation and persistence. Our data reveal the predominant influence of membrane-proximal domains in driving T cell phenotype. Notably, CD40 costimulation was crucial for fostering robust and lasting T cell responses. Furthermore, we correlated in vitro generated CAR T cell phenotypes with clinical outcomes in patients treated with CAR T therapy, establishing the foundation for a clinically informed screening approach. This work deepens our understanding of CAR T cell biology and may guide future CAR engineering efforts.

INTRODUCTION

Chimeric antigen receptor (CAR) T cells are an emerging therapeutic strategy for cancer treatment. CARs are synthetic receptors consisting of an extracellular antigen-binding domain fused to intracellular signaling domains that trigger and modulate T cell responses upon activation. The infusion of genetically engineered CAR T cells in patients guides the recognition of a target tumor antigen and promotes tumor clearance while inducing long-lasting memory immunity (*1*, *2*). To date, seven CAR T cell therapies have been approved by the Food and Drug Administration for the treatment of hematological malignancies, and there are more than a thousand ongoing clinical trials for a broad range of cancer types (*3*). Despite the potential of these therapies, they still face several challenges, including associated toxicities, poor tumor infiltration, exhaustion, and lack of T cell persistence, which have limited their clinical success in many indications (*4*).

In recent years, the search for solutions has motivated the engineering of different CAR designs that enable novel recognition and activation properties (*5*). In particular, the essential role of intracellular signaling elements in orchestrating cellular responses and the large diversity of existing immune signaling proteins have been harnessed to expand the repertoire of CAR signaling architectures. The architecture can be defined as the choice, number, and specific arrangement (membrane proximal or distal) of signaling elements within the CAR construct. Moving beyond clinically approved CARs, which combine the signaling domains of the CD3ζ chain of the T cell receptor (TCR)/CD3 coreceptor complex and costimulatory receptors CD28 or 4-1BB, several studies have investigated the impact of making precise changes in the choice, number, and order of signaling domains (*6*–*10*) or motifs (*11*, *12*). Despite technical limitations of functional assays, which restrict the number of constructs that can be individually produced and tested, preclinical studies have identified new CAR designs with distinct antitumor properties. For instance, combining CD79A and CD40 signaling domains resulted in CARs exhibiting improved proliferation and superior in vivo antitumor activity compared to clinically approved designs (*6*). Furthermore, incorporation of CTLA4 cytoplasmic tails into a CD28-CD3ζ CAR increased its cytotoxic potential while delaying T cell activation and proinflammatory cytokine production, ultimately enhancing CAR T efficacy in a murine model of leukemia (*7*).

To further explore the vast CAR signaling domain combination space, several recent studies have designed high-throughput screening approaches to engineer CARs with distinct or enhanced functional properties. These strategies combine the use of signaling domain libraries, pooled screening, deep or single-cell sequencing, and computational tools to address challenges in CAR T cell engineering. The choice of the optimal methodology, however, poses a nontrivial task. Using different library designs and T cell platforms (primary cells or cell lines), Gordon *et al.* (*13*) and Goodman *et al.* (*14*) conducted pooled phenotypic screens through fluorescence-activated cell sorting (FACS) and deep sequencing to assess the enrichment of functional variants. Daniels *et al.* (*15*) performed arrayed screening on a subset of a CAR library, recording flow cytometry–based phenotypic information, which was followed by machine learning to predict the cytotoxicity and memory potential of a larger library of signaling architectures. Notably, our group has performed pooled functional screening of a large CAR signaling domain library and used single-cell RNA sequencing (scRNAseq) for high-throughput assessment of T cell transcriptional phenotypes (*16*).

Now, there is still limited understanding of how the architecture of a CAR translates to the functional or transcriptional phenotype of T cells. In addition, the dynamics of how these cellular phenotypes evolve over time requires further investigation, especially in a clinically relevant context such as chronic antigen stimulation, which is known to drive T cell exhaustion, a main cause of therapy

[1]Department of Biosystems Science and Engineering, ETH Zürich, 4056 Basel, Switzerland. [2]Life Science Zurich Graduate School, Systems Biology, ETH Zürich, University of Zurich, 8057 Zürich, Switzerland. [3]IBM Research Europe, Zurich, Switzerland.
*Corresponding author. Email: sai.reddy@ethz.ch (S.T.R.); rocio.castellanos@bsse.ethz.ch (R.C.-R.)

failure (*17*, *18*). Here, we systematically study the role of CAR signaling architectures on T cell activation and persistence by combining pooled functional screening of a combinatorial signaling domain library with scRNAseq. This enables the characterization of CAR T cell responses in a high-throughput manner while mimicking the early and late stages of chronic tumor stimulation through an in vitro model of CAR T cell dysfunction. Capturing different single-cell transcriptomic snapshots across time, our data reveal intriguing patterns, such as the prominent influence of domains proximal to the cell membrane in modulating T cell phenotype and the pivotal role of CD40 costimulation in driving a potent yet persistent T cell response. Furthermore, by leveraging a published scRNAseq dataset of in vitro stimulated infusion products, we linked our in vitro generated CAR T cell phenotypes to clinical outcomes in patients with acute lymphoblastic leukemia (ALL), providing an approach to bridge in vitro phenotypes with the clinical performance of CAR T cell products. Thus, our study synergizes signaling domain engineering, pooled functional screening, and scRNAseq to enhance our understanding of how CAR architecture modulates T cell antitumor potential.

RESULTS

Design of a combinatorial signaling domain library of CAR variants

To systematically investigate the impact of modifying the intracellular architecture of CARs on T cell function, we generated a combinatorial signaling domain library based on first, second, and third generation CAR designs; a classification based on the number of costimulatory domains (Fig. 1A). All CAR designs had the same extracellular domain consisting of a single-chain variable fragment (scFv) with binding specificity for the human epidermal growth factor receptor 2 (HER2), which is a tumor-associated antigen present on several solid cancers (*19*). The CD3ζ activation domain was combined with costimulatory

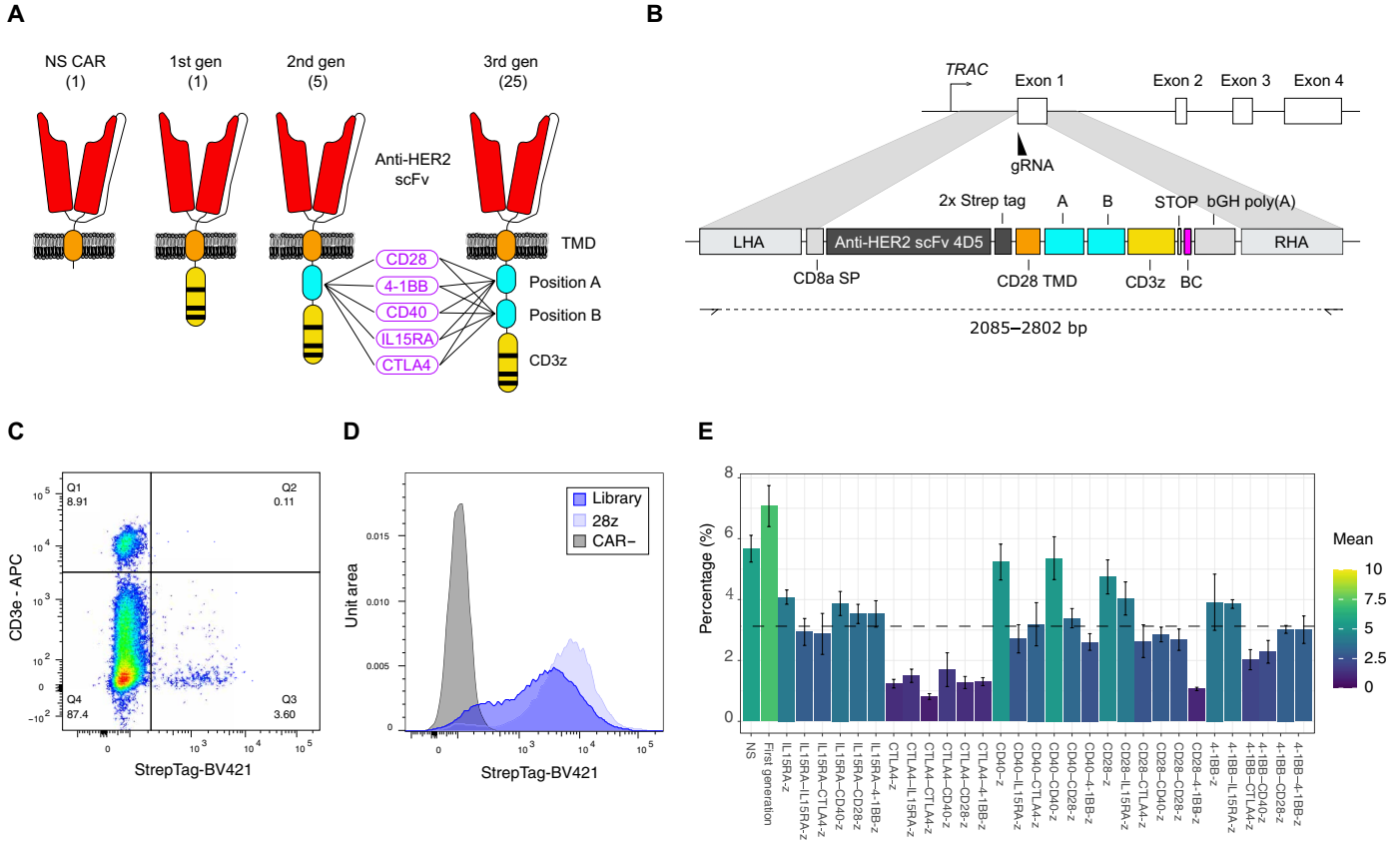

Fig. 1. Design and production of a combinatorial signaling domain library of CAR variants. (**A**) Schematic representation of the CAR library design. The library consists of second and third generation CAR designs that recombine five selected costimulatory domains in all possible combinations, a first generation CAR and a nonsignaling (NS) CAR that lacks signaling domains. When referring to domain positioning within the CAR, positions A and B denote domains located proximal or distal to the cell membrane, respectively. All variants contain an anti-HER2 single-chain variable fragment (scFv) and a CD28 transmembrane domain (TMD). (**B**) Schematic shows the targeted genomic integration of the CAR library into the *TRAC* locus of T cells. Following a CRISPR-Cas9 guide RNA (gRNA)–directed double-stranded break at the start of exon 1 of the *TRAC* locus, a dsDNA repair template having left and right homology arms (LHA and RHA) and a full CAR gene {signal peptide (SP), scFv, TMD, signaling domains and polyadenylate [poly(A)] signal} is used to induce HDR and CAR gene insertion. (**C**) Flow cytometry plot illustrating the T cell product obtained 6 days after the engineering of the CAR library into primary human T cells. Positive surface expression of a CAR (StrepTag) and negative expression of the TCR (CD3ε coreceptor) identifies correctly engineered CAR T cells. (**D**) Flow cytometry histograms display CAR surface expression profiles of 28z and the pooled library of CAR T cells after enrichment compared to unedited T cells. (**E**) Library diversity of the CAR T cell final product following enrichment and a 12-day expansion, assessed by deep sequencing of genomic DNA-amplified CAR barcodes. The dashed line represents the theoretically balanced distribution of the library. Barplot shows the mean of five biological replicates (CAR T cell products engineered from different healthy donors), and error bars represent SEM. APC, allophycocyanin; bp, base pair.

signaling domains of five different immune receptors, which cover different receptor families that are known to trigger distinct signaling pathways for modulating T cell activity. CD28 and 4-1BB [tumor necrosis factor receptor superfamily 9 (TNFRSF9)] were selected as they are the most commonly used costimulatory domains and are present in clinically approved CAR T cell therapies. In addition, we included the signaling domains of CD40 (TNFRSF5) and the IL-15 cytokine receptor alpha chain (IL15RA), which in preclinical studies have demonstrated the ability to enhance the antitumor properties of CARs (*6*, *20*, *21*). Last, CTLA4 was chosen as an example of an inhibitory receptor on T cells that still may enhance antitumor responses when incorporated into CARs (*7*). As a negative control, a nonsignaling CAR (NS-CAR) was designed, which lacks any intracellular signaling domains and is therefore unable to initiate CAR-dependent T cell activation. This results in a library with 32 different designs: 1 first generation, 5 second generation, 25 third generation CARs, and the NS-CAR as a negative control (Fig. 1A).

Next, we used CRISPR-Cas9 and homology-directed repair (HDR) to genomically integrate the CAR library into the TCR alpha chain (*TRAC*) locus of primary human T cells (Fig. 1B). Precise integration of the CAR gene into the *TRAC* locus ensures that every variant is expressed under the same transcriptional regulation while simultaneously knocking out the TCR (*22*), an appropriate setting to compare library candidates in a pooled manner. Following genome editing, engineered T cells were selected on the basis of positive surface expression of a CAR (StrepTag) and negative expression of the TCR (CD3ε coreceptor) using FACS (Fig. 1C). To verify the quality of the engineered CAR T cell product and the validity of the library controls, we first examined the CAR surface expression and cytotoxic potential of T cells engineered with the CD28 second generation CAR (28z) or the negative control NS-CAR. Both CAR T cell products displayed similar levels of CAR surface expression after enrichment (fig. S1A). Subsequently, T cell killing potential was measured by monitoring the growth curves of SKBR3 cells, a HER2-positive breast cancer cell line, following a 48-hour coculture. As expected, 28z CAR T cells were able to efficiently eliminate all tumor cells, while NS-CAR T cells were unresponsive (fig. S1B).

We next proceeded to produce a pooled library of CAR T cells including all 32 CAR variants. The surface expression of the CAR library in sorted T cells appeared to be more heterogeneous compared to the 28z CAR (Fig. 1D), indicating CAR variant-specific differences in cell surface expression. This is in particular expected for CARs containing a CTLA4 domain, where the presence of an endocytosis motif has been previously described to drive receptor recycling and degradation (further validated in fig. S2) (*23*). Targeted deep sequencing of the CAR library barcodes confirmed that all variants were expressed and could be enriched by FACS. Except for a few variants that showed a lower enrichment, most of which indeed contained the signaling domain of CTLA4, and the library variants were distributed at similar levels (Fig. 1E; CAR nomenclature is described in table S1). To validate that recombination events during the library generation were not disrupting the correct CAR-to-barcode pairing, we evaluated the correct linkage between barcodes and CAR sequences using long-read sequencing. Barcodes (91.3%) correctly paired with their corresponding CAR sequences.

Assessment of library persistence following RAS

Next, we characterized CAR signaling domain variants using in vitro repeated antigen stimulation (RAS), an experimental workflow that aims to mimic chronic antigen stimulation from tumor cells (*24*, *25*), which is associated with CAR T cell exhaustion during clinical treatment. The pooled library of CAR T cells was repeatedly challenged with HER2-expressing SKBR3 cells for 12 days. Every third day, a sample of the cocultured cells was restimulated with fresh SKBR3 cells, and their effector potential was assessed by flow cytometry based on surface expression of the degranulation marker CD107a and intracellular expression of pro-inflammatory cytokines interferon-γ (IFN-γ) and tumor necrosis factor–α (TNFα) (Fig. 2A). At an early stage of the RAS assay (day 3), the CAR T cell library showed robust effector potential as evidenced by high degranulation and cytokine production (Fig. 2B). A consistent and gradual decline of this effector phenotype was observed toward later time points, indicating that the RAS assay could effectively recapitulate the progressive exhaustion of CAR T cells. Throughout the assay, CD8 T cells seemed to lose effector potency faster than CD4 T cells. In line with this observation, the fraction of CD8 T cells consistently dropped in time in favor of CD4 T cells, which seemed to have a longer life span in the context of an in vitro RAS coculture (Fig. 2C).

On the basis of the RAS functional characterization, we observed that the library of CAR T cells reached a predysfunctional state by day 9. The antitumor potential at this stage was evidently reduced; however, T cells were still able to control tumor cell growth. To assess the persistence of the different CARs, we aimed to resolve the library diversity following a FACS-based selection of cells that remained positive for effector markers (CD107a or IFN-γ) by day 9 of the RAS assay (Fig. 2D). Targeted deep sequencing of the CAR transgenes was performed before and after FACS, and enrichment scores were computed using post-enrichment library frequencies normalized to baseline (library frequencies on day 9 before selection) for the CD8 and CD4 T cell populations. As expected, the NS-CAR was consistently depleted for every marker (Fig. 2E). Notably, the CD40 signaling domain in position A (proximal to the cell membrane) was a key driver of T cell persistence, resulting in high enrichment scores for all groups (Fig. 2E and fig. S3). However, CD40 in position B (distal from the cell membrane) showed lower enrichment scores but still promoted a proinflammatory phenotype in CD8 cells. In addition, CTLA4 in position B was enriched in $CD107a^+$ cells and thus appeared to drive a more persistent cytotoxic phenotype. CD28 and 4-1BB signaling domains induced a moderate or reduced persistence.

Single-cell transcriptional profiling resolves CAR-induced phenotypes

We next sought to further resolve the CAR-induced T cell phenotypes of the library across RAS using the multidimensional readout of scRNAseq. CAR T cell library cells were produced from two healthy donors, and transcriptomic data were generated at early, middle, and late stages of the RAS assay (days 0, 6, and 12). At each of these time points, CAR T cells were stimulated with HER2-expressing SKBR3 cells for 6 hours and then sequenced (Fig. 3A). In addition to the scRNAseq data, we performed single-cell cellular indexing of transcriptomes and epitopes (scCITEseq; a sequencing-based method capable of simultaneously quantifying cell surface proteins alongside transcriptomic data within a single-cell readout) to detect a panel of T cell surface marker proteins. Last, we also performed single-cell CAR sequencing (scCARseq) using an adapted protocol from our previous work (*16*), which enables demultiplexing of the pooled CAR library by identifying the CAR variant of each cell (fig. S4).

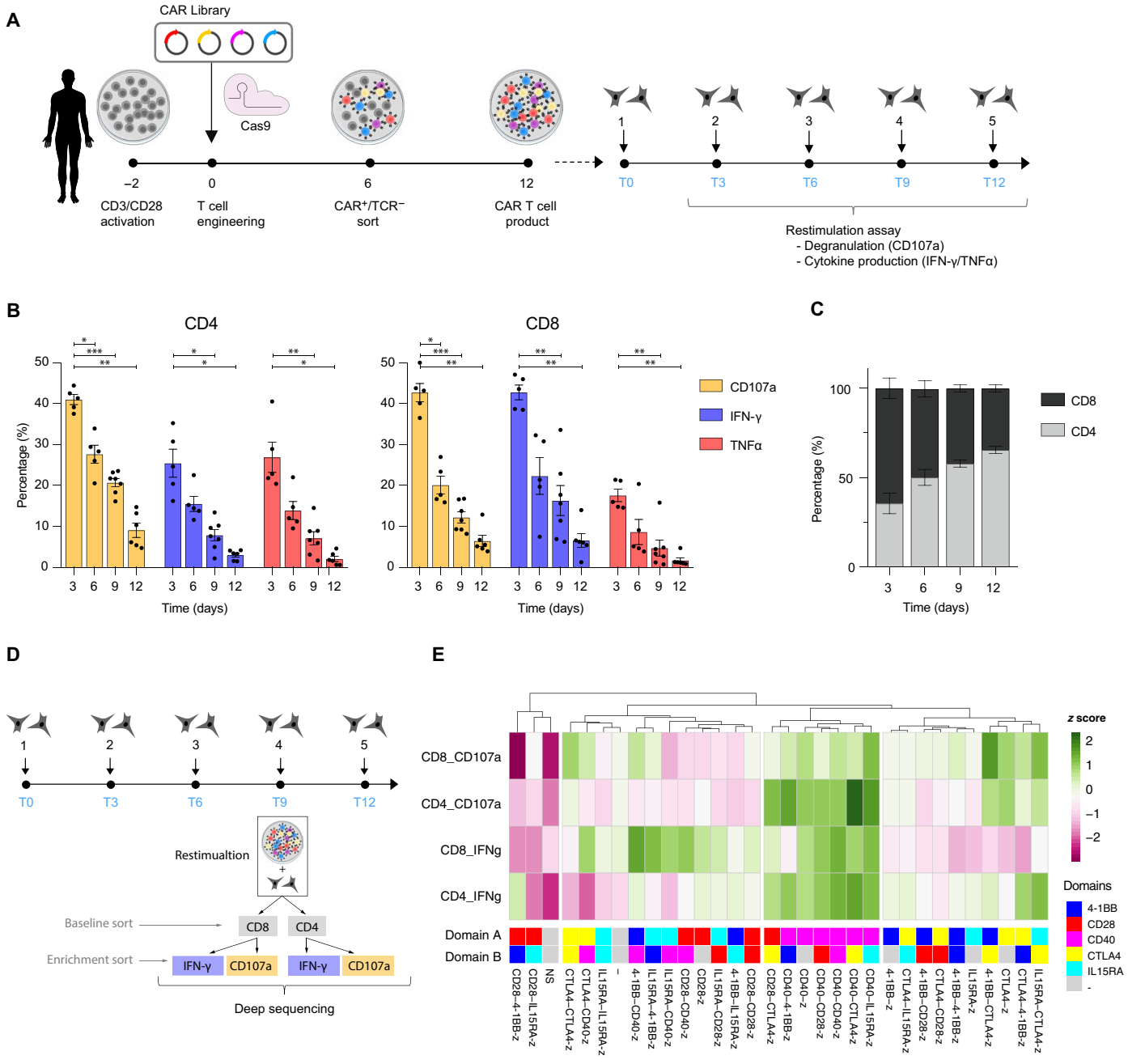

Fig. 2. Assessment of T cell dysfunction using a repeated tumor rechallenge assay identifies varying potentials among CAR architectures to promote T cell persistence. (**A**) Schematic representing the CAR library production protocol followed by a RAS assay. Twelve days after T cell engineering, a purified population of library CAR T cells was cocultured with HER2^{+} SKBR3 target tumor cells at a 1:1 effector to target (E:T) ratio. Every three days, the coculture was reset and a fraction of cells was used to assess the T cell antitumor potential. (**B**) Percentage of CD4 and CD8 cells presenting surface expression of CD107a or intracellular production of IFN-γ and TNFα at different stages of the RAS assay. Significant differences between time points were assessed using a Dunnett's multiple comparisons test with the following significance indicators: *$P < 0.05$, **$P < 0.001$, and ***$P < 0.0001$. (**C**) Percentage of CD4 and CD8 cells observed at different stages of the RAS assay. (B and C: $n = 7$, including four different donors. Error bars represent SEM). (**D**) Schematic describing the sorting strategy used to assess the CAR library cytotoxic (CD107a) and proinflammatory (IFN-γ) potential at a pre-exhausted stage of the RAS assay. Both baseline and enrichment samples, used to compute scores in (E), were sorted at day 9. (**E**) Hierarchical clustering of the CAR library according to the enrichment or depletion of variants following CD107a or IFN-γ positive selection after 9 days of RAS assay. Variants are clustered according to *z* scores, calculated based on the $\log_2$ fold change in relative library frequencies at day 9 before and after enrichment for effector markers shown in (D). CD8 and CD4 T cell compartments were analyzed separately ($n = 3$, independent biological replicates). Panels (A) and (D) were partially created with BioRender.com.

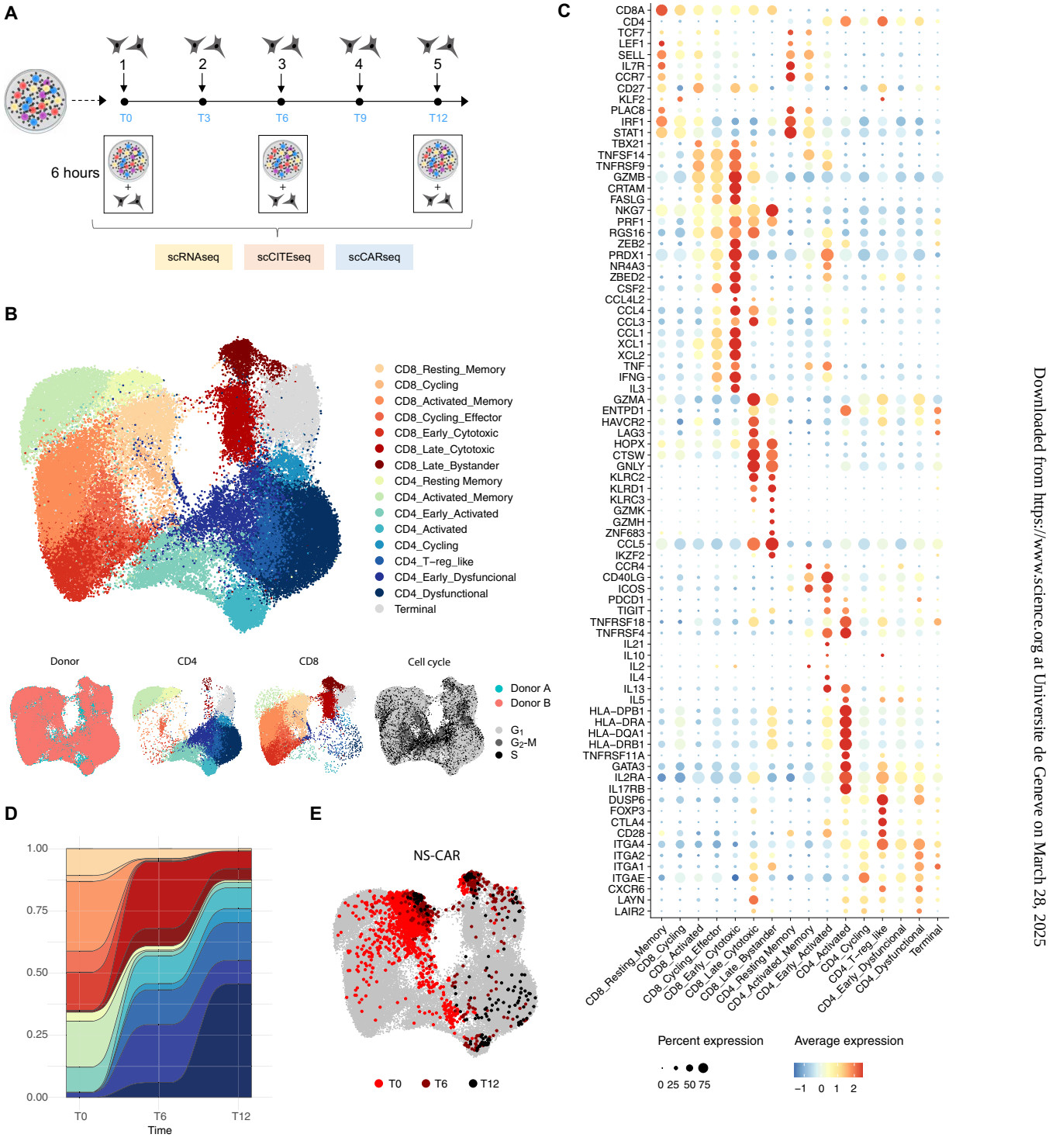

Fig. 3. Single-cell sequencing resolves and demultiplexes CAR-induced transcriptional phenotypes from pooled CAR T cell libraries during prolonged antigen stimulation. (**A**) Schematic describing the generation of single-cell data. The pooled library of CAR T cells from early, middle, and late time points in the RAS assay was stimulated for 6 hours in the presence of SKBR3 target tumor cells and then processed using scRNAseq, scCARseq, and scCITEseq. (**B**) UMAP embedding and unsupervised cell clustering of the scRNAseq data generated as described in (A). A total of 58,949 cells from two healthy donors and three time points are shown. At the bottom, UMAP embeddings are colored on the basis of donor, CD4, or CD8 annotation and cell cycle phase. (**C**) Dot plot shows the expression of a selection of differentially expressed T cell marker genes that are used to annotate the clusters described in (B). (**D**) Change in cluster representation across time points. (**E**) Distribution of cells annotated to display a nonsignaling CAR (NS-CAR) within the UMAP embedding of (B). Panel (A) was partially created with BioRender.com.

Single-cell sequencing and data processing resulted in a total of 62,934 annotated CAR T cells across the three different time points, with full coverage of the CAR library across every time point and donor. An additional random subsampling of abundant variants was performed to ensure a more balanced representation of all library candidates, allowing for a more accurate and unbiased assessment of the phenotypic diversity. This resulted in 58,949 cells, which were used for downstream phenotypic analysis (fig. S5). The lack of correlation between the expression of TCR variable genes across CAR variants, time points, or donors validated the presence of sufficient clonal diversity in our library (fig. S6). Dimensionality reduction by uniform manifold approximation and projection (UMAP) and unsupervised cell clustering separated cells into 16 different clusters (Fig. 3B). Annotation of the clusters was based on CD4 and CD8 expression, cell cycle phase prediction, and differential gene and surface expression of key T cell marker genes (Fig. 3C and fig. S7); both CD4 and CD8 T cell subsets presented a resting memory cluster characterized by the expression of TCF7, CCR7, LEF1, and SELL genes and protein surface expression of CD45RA and CD62L. The CD8 memory cluster then progressively transitioned into activated and effector phenotypes characterized by the increased expression of activated (TNFRSF9, TBX21, and ZBED2), cytotoxic (GZMB, PRF1, and FASLG) and proinflammatory genes (CRTAM, IFNG, TNF, CSF2, XCL1, and XCL2) and eventually into a late cytotoxic phenotype characterized by the expression of late effector differentiation genes such as HOPX, ENTPD1, LAG3, HAVCR3, and GNLY. Cytotoxicity was also evidenced by the increased surface detection of HER2 on CAR T cells as a result of trogocytosis, a process by which there is a unidirectional transfer of plasma membrane and associated surface proteins from target cells to effector lymphocytes (fig. S7C) (*26*). Last, a CD8 cluster was observed that presented a CAR-independent, bystander T cell activation signature. This cluster exhibited transcriptomic hallmarks of T cell activation (GNLY, CCL5, and several KLR genes), previously described in CAR-negative T cells from patient samples during CAR T cell treatment, which are distinct from those seen in CAR T cells (*27*). This could be attributed to the effect of the cytokine storms and the cell killing environment on unstimulated T cells. Likewise, the CD4 memory cluster also transitioned into activated and more differentiated phenotypes evidenced by the expression of activation genes such as CD40LG, IL2RA, ICOS, TNFSF14, TNFSF, and IL17RB and a broad range of cytokines. This activated phenotype later transitioned into a rather dysfunctional phenotype and a regulatory T cell (T_{reg})–like cluster characterized by the expression of FOXP3 and CTLA4. Last, a mixed CD4 and CD8 cluster, high in mitochondrial gene expression, was annotated as a terminal phenotype.

The progression of T cell phenotypes from a memory and early activation state, through a potent effector phenotype, to a late, less functional state correlated with the scCITEseq data for surface expression of early, middle, and late T cell activation markers (fig. S7B), RNAvelocity analysis (fig. S8) and the time points at which the samples were collected (Fig. 3D and fig. S9A). As previously observed, the CD8 compartment was markedly reduced through RAS progression in favor of a growing ratio of dysfunctional CD4 CAR T cells. The absence of CD8 cells presenting a terminally exhausted phenotype and the drop in the overall number of T cells in late cocultures suggest the death of CD8 cells following their terminal effector differentiation.

Having resolved the recorded T cell phenotypes, scCARseq enabled us to demultiplex the CAR library identity and investigate how different CAR signaling architectures can drive distinct T cell responses upon both initial and RAS. First, we examined the T cell phenotypes of the NS-CAR through time (Fig. 3E). As expected, the lack of CAR signaling domains resulted in nonactivated T cells that remained in a resting memory phenotype at early and even late time points. As the RAS assay progressed, a fraction of cells transitioned toward a CD8 bystander T cell activation phenotype markedly distinct to that induced by CAR signaling. A CD4 bystander effect appears to overlap slightly with a dysfunctional phenotype. Cluster enrichment of CD4 and CD8 cells across time points for the rest of the library variants indicated that every other CAR was able to trigger T cell activation, as evidenced by the lack of cells presenting a resting memory phenotype (fig. S9B).

Role of signaling domain combinations in early activation of CAR T cells

To understand how signaling domain combinations shape the early activation of T cells, we examined transcriptional phenotypes after 6 hours of tumor coculture. For both CD8 and CD4 subsets, we could observe the separation of cells across a T cell differentiation axis. When ordering cells according to a predicted pseudotime, the annotated clusters indeed followed such a trajectory, evolving from a resting memory to a potent effector phenotype (fig. S10). The enrichment of CAR variants across these clusters can therefore reveal differences in early activation signatures triggered by the different CARs. For the CD8 cell compartment, the presence of the CD40 domain in position A appeared to be the main driver of a fast and potent effector phenotype, as all CD40 variants (except CD40–4-1BB) presented the highest percentage of cells within the effector and cytotoxic clusters (Fig. 4A). On the other hand, 4-1BB containing CARs, while still activated, appeared to trigger a less potent but stronger effector memory-like phenotype. Notably, CD4 cells showed a different trend; for example, CTLA4-containing CARs appeared to drive the strongest CD4 activation and differentiation, while CD40, CD28, and 4-1BB retained an overall CD4 effector memory phenotype.

In addition to cluster enrichment, we used single-cell gene set scoring to further resolve the activation signatures based on the simultaneous expression of several marker genes. The CD8 effector phenotype was assessed for its cytotoxic and proinflammatory potential, and a memory phenotype score was computed for all cells (Fig. 4B). On the basis of these scores, in silico sorting of cells was performed to assess the different CAR library variants by their enrichment in such phenotypes. Using the NS-CAR to set a baseline threshold, we then investigated the impact of CAR signaling domain composition on the appearance of each of these phenotypes (Fig. 4C). As described previously, all CAR constructs were able to trigger a strong cytotoxic phenotype (40 to 70% of CD8 cells); however, once again, the CD40 domain in position A appeared to drive a particularly high cytotoxicity that was enhanced when the CD40 domain is repeated. This pattern is even more notable when examining the proinflammatory signature. CD40 in position A also resulted in the most powerful proinflammatory phenotype that appears to be slightly restrained when incorporating 4-1BB or CTLA4. The second generation 28z CAR, as expected, induced several of the most potent cytotoxic and proinflammatory signatures, serving as validation of our results. Last, the memory phenotype signature

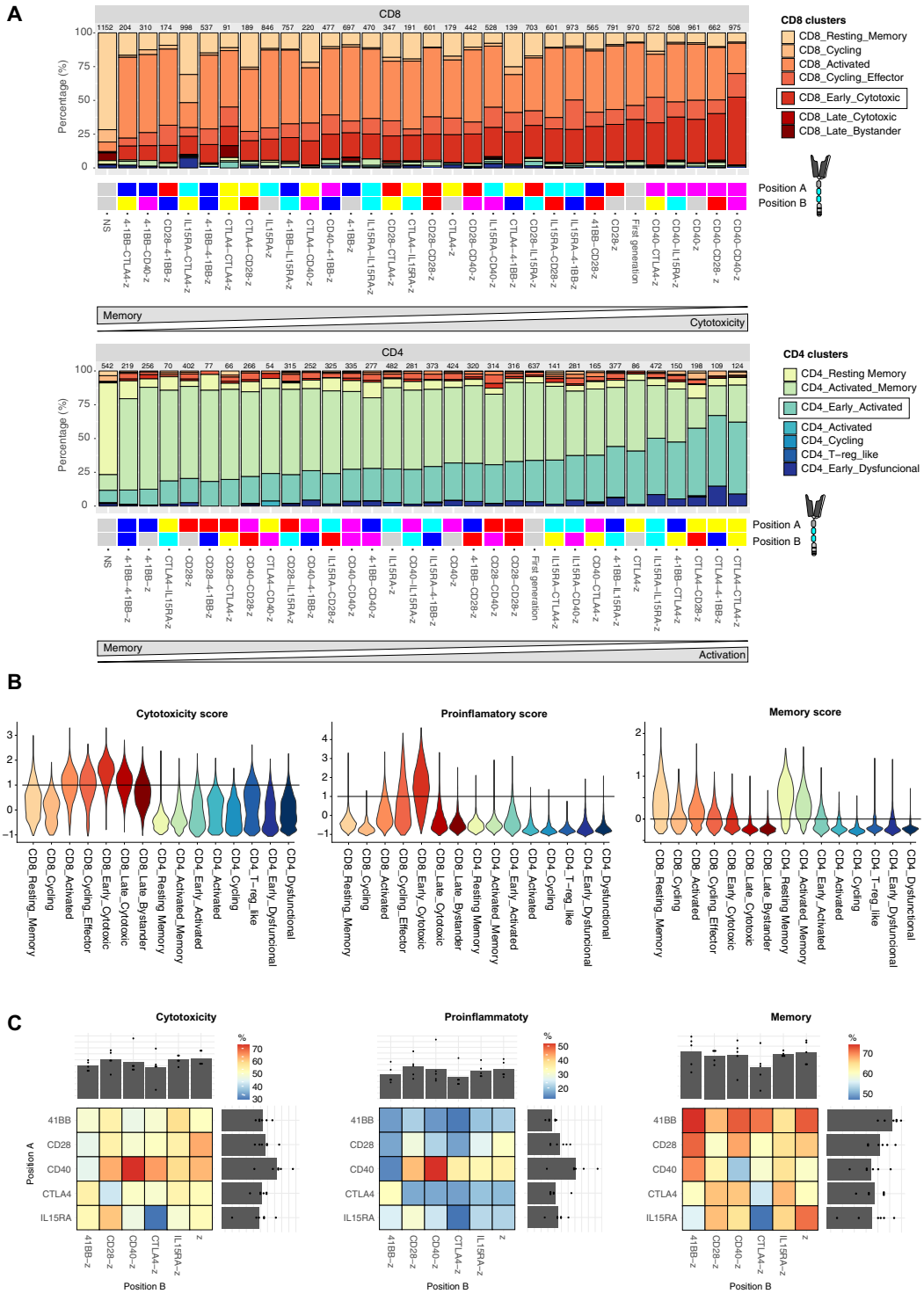

Fig. 4. CAR signaling architecture modulates T cell early activation phenotypes along a memory-effector differentiation axis. (**A**) Cluster enrichment observed for the different CAR T cell variants following 6 hours of tumor coculture. CD8- and CD4-annotated cells are shown in different plots, and variants are ordered (right to left) by the enrichment in the cluster highlighted with a black box. Under each bar plot, a heatmap describes the intracellular domain combination of the library candidates. The number of cells used to define the cluster distribution is reported at the top of each bar. (**B**) Distribution of single-cell gene-set scores across the different clusters described in Fig. 3. A horizontal line determines a threshold at which cells are considered to be positive for each given score. (**C**) Heatmaps show the percentage of cells with a positive score based on the thresholds described in (B) following 6 hours of tumor coculture. Each heatmap separates variants based on the CAR signaling domains in position A (proximal to the cell membrane) or position B (distal from cell membrane). In addition, bar plots at the top and right-hand side of the heatmap compile the frequencies for all variants presenting a given domain in the different positions. Heatmaps for cytotoxicity and proinflammatory scores only include CD8 cells, while the memory score includes both CD4 and CD8 cells.

seemed to be highly enriched in 4-1BB–containing CARs, once again aligning with previous studies (*28*, *29*).

CAR costimulation can modulate long-term T cell persistence

A common limitation often faced by CAR T cell therapies is the transient persistence of T cells, ultimately resulting in their inability to control tumor growth and disease progression (*4*, *30*). Identifying CAR design features that promote a more persistent phenotype is of substantial value. To address this, we next leveraged the RAS assay to study the progression of T cell phenotypes across the CAR library. The scRNAseq data of CAR T cells from middle and late time points in the RAS assay were separated by CD4 and CD8 annotation and reclustered to further resolve the RAS late-stage phenotypes.

Among the CD8 compartment, we observed two clusters, annotated as proinflammatory (CRTAM, IFNG, and CSF2) and cytotoxic (PRF1, GZMB, GNLY, and IL2RA) that still present effector potential (Fig. 5, A to C). Excluding a resting memory-associated cluster, the remainder of the clusters start to lose the expression of key effector marker genes, reaching a dysfunctional and subsequent terminal phenotype that ultimately leads to cell death. Using the enrichment of proinflammatory and cytotoxic clusters at a RAS late time point (12 days) as a marker for persistence, we observed that CD40, mainly in position A, appeared to be a key domain for long-term persistence (for both proinflammatory and cytotoxicity phenotypes). 4-1BB and CTLA4 promoted a late-stage cytotoxic, but not a proinflammatory, phenotype. IL15RA and CD28, on the other hand, had the largest percentage of cells already transitioning into a dysfunctional phenotype (fig. S11).

Another feature to take into consideration within the CD8 T cell compartment is the decline in CD8 cell numbers over time. As previously mentioned, this reduction in the CD8/CD4 ratio appears to correlate with terminal effector differentiation, ultimately leading to cell death of only CD8 cells. A faster drop in CD8/CD4 ratio can therefore be associated with a lack of persistence. By combining CD8/CD4 fold change (fig. S12) with the enrichment in the late effector clusters, we can obtain a more comprehensive persistence score (Fig. 5D). On the basis of this, CD40 once again proves to be the signaling domain that induces the most persistent phenotype, followed by CTLA4.

Among the CD4 subset, another two main functional clusters, a proinflammatory T helper 1 (T_H1) (TBX21, CRTAM, IFNG, and GZMB) and a polyfunctional T_H2 cluster (GATA3, IL4, IL5, and IL13), were identified in addition to other cycling, T_{reg}-like and dysfunctional clusters (Fig. 5, E and F). The T_H1 and T_H2 signature was also confirmed by gene set scoring (Fig. 5G). Cluster enrichment was then used to evaluate the persistence of CD4 CAR T cell variants. CD40 consistently drove the most persistent proinflammatory signature by being the most enriched in the T_H1 cluster, while CTLA4 and 4-1BB promoted a T_H2-enriched persistent phenotype (Fig. 5H). On the other hand, CD28-containing CARs were consistently the most enriched variants in the dysfunctional cluster, suggesting once again that CD28-containing CARs are prone to induce poor persistence (fig. S11).

Mapping CAR library in vitro generated phenotypes to clinical outcomes in patients with ALL

Despite the indispensable contributions of in vitro assays to CAR T cell research, translating these findings from bench to bedside remains very challenging. To put our findings in a more clinically relevant context, we developed a strategy to map the in vitro generated phenotypes observed in our CAR library T cell product onto scRNAseq data from in vitro stimulated patient-derived CAR T therapy infusion products (tisa-cel; anti–CD19-BBz CAR), which were used to treat 12 pediatric and young adult patients with ALL (Fig. 6A) (*31*). As expected, the reference annotation transfer predicted an enrichment of resting memory clusters among cells from unstimulated infusion products (Fig. 6B and fig. S13, A and B). In addition, a fraction of unstimulated cells was predicted to exhibit a CD4 early dysfunctional or terminal phenotype. Following 6 hours of in vitro stimulation resulted in the transition of a large fraction of the cells in the infusion products to early CD4- and CD8-activated CAR T cell phenotypes. Those cells that retained a resting phenotype likely represent CAR-negative cells within the infusion product. The gene expression patterns of selected marker genes across the predicted cluster annotations validated the accurate label transfer, as similar gene expression signatures were maintained compared to the reference dataset (fig. S13C).

Next, we sought to identify any correlation between the enrichment of CAR-induced phenotypes in infusion products following in vitro stimulation and clinical response in patients with ALL (Fig. 6, C and D, and fig. S13, D and E). First, we observed that nonresponders (NR) presented a reduced enrichment in activated or cytotoxic CD8 phenotypes, as well as in the CD4-activated memory phenotype, compared to both complete responders (CR) and relapsed (RL) patients. Within the CD8 compartment, CR and RL patients exhibited similar levels of resting memory cells. However, CR patients appeared to be enriched in the early cytotoxic phenotype, while RL patients had a higher enrichment of the activated phenotype (Fig. 6C). Last, CR patients also seemed to be enriched in the CD4-activated memory phenotype compared to RL patients (Fig. 6D). Despite the lack of statistical significance of these observations due to the small sample size and high variability among patients, enrichment in CD8 early cytotoxic and CD4-activated memory phenotypes appears to correlate with better clinical responses in patients with ALL. Assigning a score to our library candidates based on their enrichment in these phenotypes further suggests that CARs containing the CD40 signaling domain, particularly in position A, may trigger T cell phenotypes that are more likely to perform successfully in an ALL clinical setting (Fig. 6E).

DISCUSSION

Domain recombination has been pivotal in the evolution of signaling networks, operating on the principle that the function of a protein domain is modular and can promote new functions when embedded differently within a cellular network (*32*). As a product of rational domain recombination, CARs can be further optimized through additional signaling domain rearrangements. Despite the remarkable progress in the field of CAR T cell engineering (*5*, *33*), considerable gaps persist in understanding how changes in the CAR signaling architecture affect resulting T cell phenotypes and their therapeutic potential. In particular, costimulatory domains have proven to be key in providing CAR T cells with essential properties for clinical efficacy, but the impact of changing the type, number, and order of costimulatory domains has yet to be systematically characterized. In this study, we bridge these gaps by combining the use of a combinatorial CAR signaling domain library, pooled screening assays, and scRNAseq to systematically study the dynamics governing CAR-induced phenotypes at high resolution.

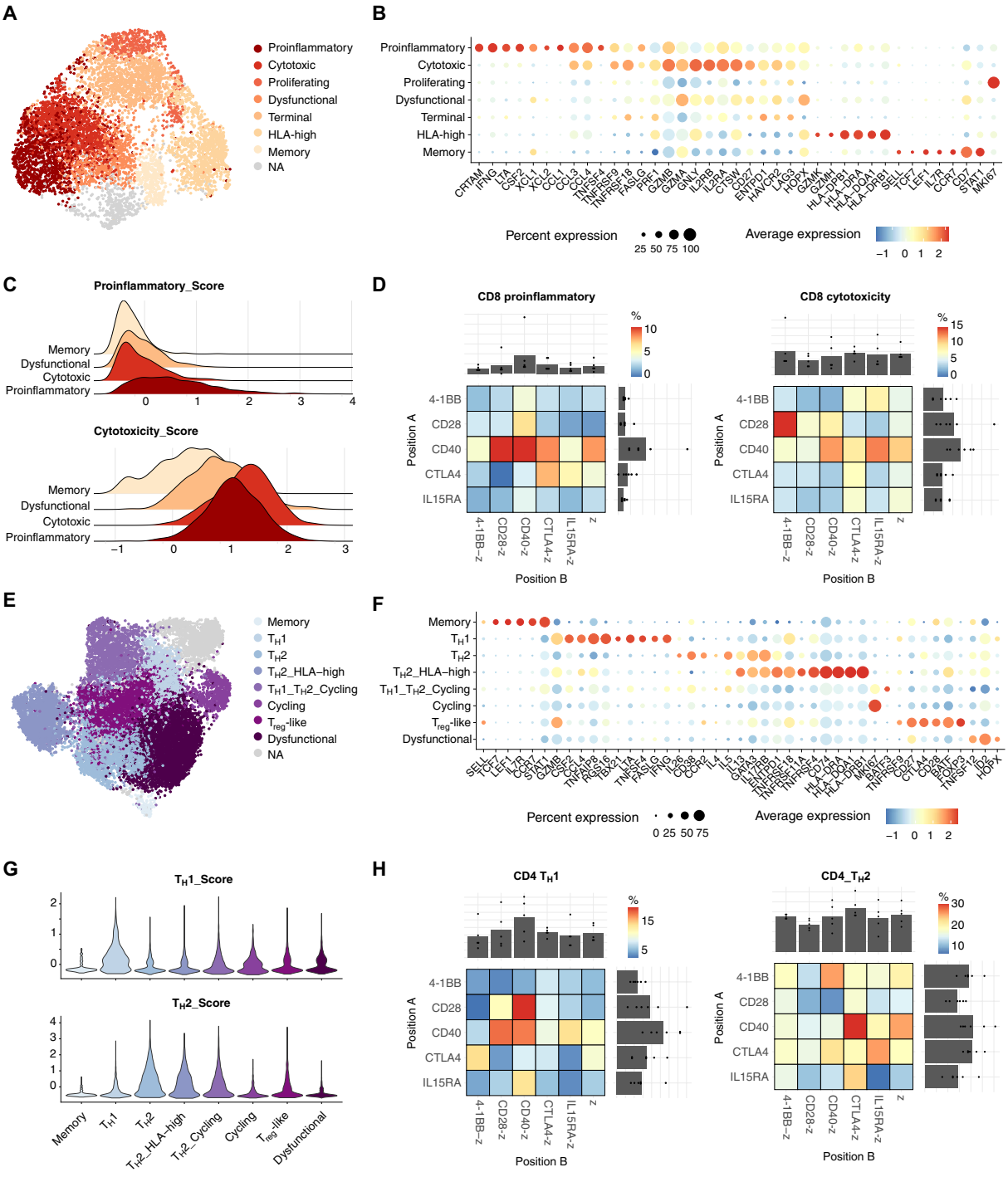

Fig. 5. CAR costimulation modulates long-term persistence during RAS. (**A**) UMAP embedding and unsupervised cell clustering of CD8 annotated cells at days 6 and 12 in the RAS assay. Cluster annotated as NA includes misannotated cells presenting a CD4-specific phenotype. (**B**) Dot plot shows the expression of a selection of differentially expressed T cell marker genes, used to annotate the clusters described in (A). (**C**) Distribution of single-cell gene-set scores across relevant clusters in (A). (**D**) Heatmaps show the enrichment of CD8 cells in the proinflammatory or cytotoxic clusters at a late time point in the RAS assay (12 days). The enrichment is corrected by the CD8/CD4 ratio fold change from day 0. Each heatmap separates variants based on the CAR signaling domains in position A (proximal to the cell membrane) or position B (distal from the cell membrane). In addition, bar plots at the top and right-hand side of the heatmap compile the frequencies for all variants presenting a given domain in the different positions. (**E**) UMAP embedding and unsupervised cell clustering of CD4 annotated cells at days 6 and 12 in the RAS assay. Cluster annotated as NA includes misannotated cells presenting a CD8-specific phenotype and dying cells with high mitochondrial gene expression. (**F** and **G**) Same as (B) and (C) but for clusters in (E). (**H**) Heatmaps show the enrichment of CD4 cells in the T_H1 or T_H2 clusters at a late time point in the RAS assay (12 days). Each heatmap separates variants based on the presence of CAR signaling domains in position A or position B. In addition, bar plots at the top and right-hand side of the heatmap compile the frequencies for all variants presenting a given domain in the different positions.

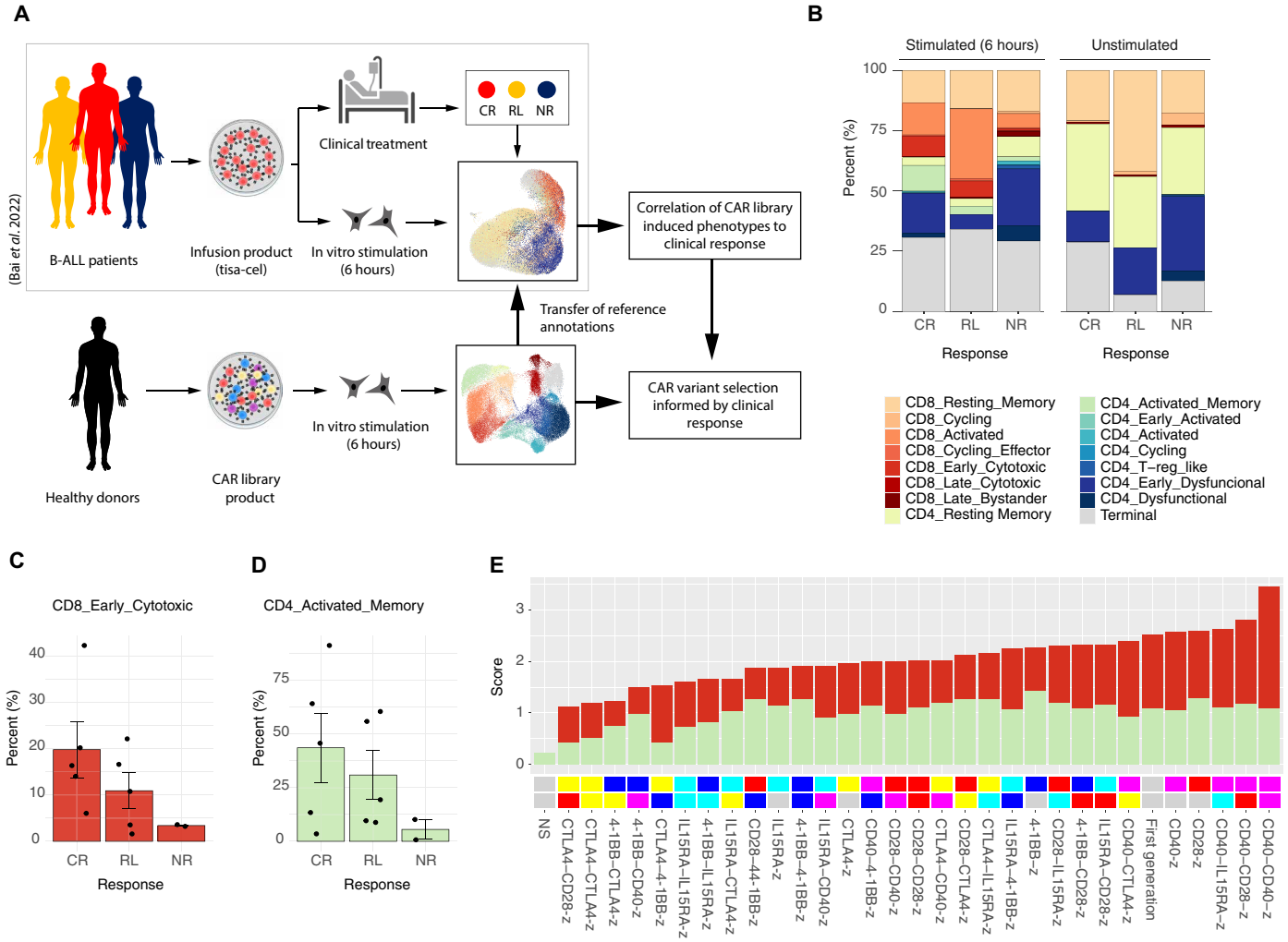

Fig. 6. Enrichment in CAR-specific in vitro generated phenotypes correlates with clinical outcomes in patients with ALL treated with CAR T therapy and can be used to inform CAR library screening. (**A**) Schematic overview of the experimental design. The in vitro phenotypes observed in our CAR library T cell product were used as a reference to annotate scRNAseq data from in vitro stimulated patient-derived CAR T therapy (tisa-cel) infusion products, generated by Bai *et al.* (*31*). Patient clinical response data were then used to correlate the enrichment in CAR library-generated phenotypes with the clinical outcomes of CAR T cell therapy. This approach enables clinically informed selection of CAR variants for further development. (**B**) Enrichment analysis of predicted cluster annotations for in vitro stimulated or unstimulated patient-derived infusion products according to their response to CAR T cell treatment. (**C** and **D**) Difference in predicted cluster enrichment within CD8 (C) or CD4 (D) clusters, across clinical response groups for patient-derived infusion products following 6 hours of in vitro stimulation. Each dot represents an individual patient, with bar plots showing the mean and error bars representing the SEM. Statistical analysis was performed using the Kruskal-Wallis test followed by Dunnett's multiple comparisons test, revealing no significant differences between treatment groups. (**E**) Relative enrichment of the phenotypes associated with CR, CD8 early cytotoxic, and CD4-activated memory phenotypes is shown across CAR library variants following 6 hours of stimulation. CAR variants are ordered according to the sum of a computed score for each cluster. Under the bar plot, a heatmap describes the intracellular domain combination of the library candidates. CR, complete response; RL, relapse; NR, no response; ALL, acute lymphoblastic leukemia. Panel (A) was partially created with BioRender.com.

We evaluated the impact of recombining five immune-receptor signaling domains, resulting in a 32-candidate CAR library that revealed architecture-specific patterns. While all CAR designs were capable of eliciting a T cell activation response, the incorporation of CD28 or 4-1BB domains replicated known phenotypic features associated with these domains (*28*, *29*, *34*); CD28 induced a potent but less persistent T cell activation, while 4-1BB promoted an effector memory phenotype. In parallel comparisons with benchmark CARs, insights into three additional domains were observed. CD40 consistently distinguished itself by triggering the most potent and persistent T cell responses. This aligns with previous findings indicating that CARs combining the signaling domains of MyD88, CD79A, or CD28 with CD40 exhibit superior proliferation and antitumor activities in preclinical tumor xenograft mouse models (*6*, *20*, *35*). Moreover, CD40-containing CARs were selected among the top candidates when performing pooled screens of two CAR libraries (*13*, *14*), further highlighting the role of this domain in enhancing CAR signaling.

CTLA4, recognized as an inhibitory receptor on T cells, when embedded in the CAR signaling architecture resulted in potent CARs capable of promoting a robust T cell response, particularly among the CD4 compartment, with a persistent cytotoxic phenotype. Despite

the inhibitory effect of CTLA4 signaling (*23*), our findings align with recent research reporting that the addition of CTLA4 cytoplasmic tails to a 28z CAR led to increased cytotoxicity and reduced production of pro-inflammatory cytokines (*7*). Despite its previous association with enhancing T cell antitumor potential (*21*), the IL15RA cytoplasmic domain did not seem to provide impactful T cell costimulation among the variants. The reduced size of its intracellular domain, coupled with the central role of its extracellular portion in carrying out its molecular function (*36*), suggests that the IL15RA domain may act as a molecular spacer within the CAR architecture.

With regard to domain positioning, our study also revealed distinctive patterns. In agreement with prior research that addressed the impact of altering the positioning of domains within the CAR (*37*–*39*), we observed that domains located closer to the cell membrane exhibited a dominant effect on phenotype. For instance, CD40 and 4-1BB, respectively, induced a distinct polarization toward effector or memory phenotype mainly when present in a membrane-proximal position. Nevertheless, domains in a more distal position continued to exert influence on phenotype, seemingly producing an additive effect. For example, CD40-z demonstrated a potent cytotoxic and pro-inflammatory phenotype, further potentiated in CD40–CD40-z but moderated in CD40–4-1BB-z, favoring a more memory-like phenotype. Despite these general observations, the mechanistic complexity associated with the introduction of domain rearrangements within a signaling network is far more sophisticated and highly dependent on the nature of the domains used. For example, CTLA4 displayed a more prominent role in promoting cytotoxicity when situated in a membrane-distal position. This observation, also suggested by Zhou *et al.* (*7*), may be linked to the role of its endocytosis motif in receptor recycling. This mechanistic feature could benefit from distal positioning while distancing CTLA4 inhibitory signaling from the dominating membrane-proximal position.

The enormous complexity associated with rewiring signaling networks highlights the value of conducting systematic studies of CAR signaling domain rearrangements. In addition, the diversity of the CAR signaling domain combination space requires high-throughput approaches that enable parallel comparisons of multiple architectures. Pooled screening of CAR libraries combined with scRNAseq provides such a high-throughput approach (*13*, *14*, *16*, *40*). An exciting frontier of this field is the integration of CAR libraries with machine learning, as previously demonstrated by Daniels *et al.* (*15*). Machine learning–guided CAR T cell engineering may further elucidate mechanistic nuances of signaling domains and enable novel CAR designs. The compact yet systematic design of our library, combined with the comprehensive and high-resolution data generated in this study, may provide training data for machine learning models that are able to decipher the rules of CAR signaling.

While our study provides valuable insights into the intricate landscape of CAR signaling and its impact on T cell phenotypes, we acknowledge certain limitations and outline future perspectives. In the context of pooled screens, the unavoidable bystander effect resulting from paracrine signaling poses logical concerns. Despite this limitation, the inclusion of a NS-CAR as a negative control allowed us to evaluate the impact of this paracrine effect in overall T cell phenotype, which identified bystander transcriptional hallmarks (*27*) distinct to those induced by CAR signaling, and stressed the importance of incorporating these controls in pooled library assays. In addition, ensuring that libraries are well-balanced is crucial, as imbalances in cell numbers can affect confidence in the conclusions drawn. Second, reproducing a clinically relevant T cell activation context poses a considerable challenge. In vitro coculture lacks the cellular heterogeneity, tumor microenvironment, and anatomical barriers encountered in real clinical scenarios. While in vivo settings attempt to address some of these challenges, human tumor xenograft mouse models in immunocompromised mice often also fall short in replicating clinical conditions. Our choice of using ex vivo RAS provided extensive phenotypic characterization of CAR signaling in a simplified setup mimicking the clinical challenge of CAR T cell dysfunction following chronic antigen exposure. Despite this, the limited understanding of the correlation of CAR T cell phenotypes with clinical outcomes still makes it difficult to speculate which variant could exhibit better clinical performance, necessitating further functional validation (*41*).

To address this gap, we performed a computational analysis that bridges in vitro phenotypic readouts with clinical responses by leveraging a unique dataset published by Bai *et al.* (*31*), which recorded scRNAseq data from in vitro stimulated infusion products from patients with ALL treated with CAR T therapy (tisa-cel). By mapping the phenotypes triggered by our library of CAR candidates to the Bai *et al.* (*31*) dataset, annotated with clinical outcomes, our analysis provides a CAR library screening approach informed by clinical response to CAR T cell treatment. While our analysis does not substitute for direct experimental validation in clinically relevant models, and transcriptomic similarities between in vitro data and clinical data do not guarantee comparable behavior in a clinical setting, this approach represents a valuable first example of a transcriptomic data-driven selection tool that can accelerate CAR library screening for particular clinical indications. Although this screening approach is currently constrained by the limited availability of these datasets (in vitro stimulated patient-derived CAR T cell scRNAseq), it underscores its value and the need for generating more datasets of this nature to be able to further develop screening tools aiming at overcome the gap between preclinical models and clinical performance.

MATERIALS AND METHODS

Library cloning

The CAR library was cloned using a type II restriction enzyme cloning strategy as previously described (*42*). A backbone plasmid containing an anti-HER2 first generation CAR gene (composed of a CD8α secretion peptide, a Herceptin-derived scFv (4D5), two Strep tags, CD28 hinge and transmembrane domains, the CD3ζ cytoplasmic region, and a bGH polyA sequence) flanked by *TRAC* locus-specific homology arms was generated. In addition, a cloning cassette with inverted Aar I sites was introduced between the transmembrane domain and the CD3ζ sequence. Last, a 3′ untranslated region (3′UTR) barcode sequence was added using an overhang polymerase chain reaction (PCR) and recircularization strategy. Synthetic gene fragments containing the cytoplasmic sequence of CD28, 4-1BB, CD40, IL15RA, and CTLA4 genes were generated (Twist Bioscience) with different sets of flanking sequences containing an Aar I recognition site that allows for the ligation of a defined number and order of domains within the CAR backbone. Domain sequences were individually amplified, digested with Aar I (Thermo Fisher Scientific; 4 hours, 37°C), and ligated into the previously digested backbone plasmid using a T4 ligase (NEB; 30 min, 37°C). For each library candidate, the ligated plasmids were transformed into *Escherichia coli*

DH5α cells, purified, and sequence-verified using Sanger sequencing. The NS-CAR and the first generation CAR were independently cloned using deletion Q5 mutagenesis. Last, all library candidate plasmids were pooled at a 1:1 ratio.

Primary human T cell isolation and culture

Buffy coats from healthy donors were acquired through the Blutspendezentrum Basel (University of Basel). All participating volunteers provided written informed consent in accordance with the general guidelines approved by Swissethics (Swiss Association of Research Ethics Committees). Peripheral blood mononuclear cells were isolated using a Ficoll-based density gradient and stored in liquid nitrogen until needed. Immediately after thawing, negative selection of T cells was performed using the EasySep human T cell isolation Kit (STEMCELL Technologies) and cultured in X-VIVO 15 medium (Lonza) supplemented with 5% fetal bovine serum (FBS), 50 μM β-mercaptoethanol, Normocin (100 μg/ml; Invivogen), and IL-2 (100 U/ml; PeproTech), referred to as T cell growth medium.

Primary human T cell genome editing

Primary human T cells were engineered to integrate a CAR gene into the *TRAC* genomic locus using CRISPR-Cas9 genome editing. Double-stranded DNA HDR template and Cas9 ribonucleoprotein (RNP) were prepared as previously described (*16*). T cells were activated using Human T-Activator CD3/CD28 Dynabeads (Thermo Fisher Scientific) at a 1:1 cell/bead ratio in T cell growth medium. After 48 hours, beads were magnetically removed, and cells were electroporated using the Lonza 4D electroporation system. To do this, 1×10^6 cells were washed once in phosphate-buffered saline (PBS), resuspended in 20 μl of P3 nucleofection buffer (Lonza) containing 1.2 μl of Cas9 RNP mix and 0.4 μg of double-stranded DNA HDR template, and electroporated using the EH-115 program. After electroporation, cells were immediately recovered in 150 μl of T cell growth medium. For each batch of CAR library T cells, at least 1×10^7 T cells were engineered to achieve sufficient clonal diversity across all candidates.

Cell line culture

SKBR3–green fluorescent protein (GFP) cell line was cultured in Dulbecco's modified Eagle's medium (Gibco) supplemented with 10% FBS, 1% penicillin-streptomycin (Gibco), and Normocin (100 μg/ml; Invivogen).

CAR T cell staining and cell sorting

Flow cytometry was used to analyze and select correctly engineered CAR T cells based on the positive staining of a StrepTag located in the extracellular portion of the CAR and the lack of expression of the TCR complex. A two-step staining strategy was used, initially using a biotinylated anti-Strep tag antibody (table S3), followed by a combination of streptavidin-BV421 conjugate and CD3ε-allophycocyanin antibody (table S3). T cells were washed in FACS buffer (PBS, 2% FBS, and 1 mM EDTA) and then incubated in FACS buffer containing the antibody mix for 20 min. Cells were then washed again and analyzed using a Fortessa LSR flow cytometer (BD) or sorted using a FACSAria Fusion (BD).

Deep sequencing of CAR libraries

The diversity of library CAR T cells was determined using deep sequencing. Genomic DNA from 5000 to 50,000 CAR-expressing T cells was extracted using Quick Extract (Lucigen) and used as the template for a two-step PCR strategy. In a first PCR reaction, primers F1 and R1 (table S2) were used to amplify a region of the CAR gene [2000 to 2500 base pairs (bp)], which confirmed the CAR integration into the *TRAC* locus. Following a 0.6X SPRIselect bead DNA cleanup (Beckman Coulter), the DNA product was used as a template for a second PCR reaction using primer mix F2 and R2 (table S2). This amplified a 261-bp sequence in the CAR 3′UTR region that contained the barcode sequence, which determines its library identity. The resulting amplicons were purified using a 1.2X to 0.6X double-sided SPRIselect bead DNA cleanup (Beckman Coulter), prepared for sequencing using a KAPA HyperPrep kit (Roche), and sequenced on an Illumina MiSeq system. Sequencing data analysis was performed using the Biostrings package in R.

Long amplicon sequencing of TRAC locus-integrated CAR transgene

Genomic DNA from 5000 to 50,000 CAR-expressing T cells was extracted using Quick Extract (Lucigen) and used as the template for the amplification of *TRAC* locus-integrated CAR transgene using primers F1 and R1 (table S2). The resulting PCR product was then cloned using the Zero Blunt TOPO PCR Cloning Kit (Thermo Fisher Scientific). Individual amplicons were then sequenced using Sanger sequencing. The correct pairing of barcodes with CAR sequences was assessed using the Biostrings package in R.

In vitro RAS

To simulate a chronic antigen stimulation, CAR T cells were repeatedly cocultured with the HER2-expressing tumor cell line SKBR3. On day 14 (12 days after bead removal and T cell engineering), T cells were cocultured with SKBR3-GFP cells at a 1:1 effector to target (E:T) ratio in CAR media supplemented with of IL-2 (30 IU/ml). Every 3 days, cells were counted using a hemocytometer, and new SKBR3-GFP cells were added to readjust the coculture to a 1:1 E:T ratio.

Degranulation and cytokine production assay

To assess the effector potential of cocultured CAR T cells, we measured degranulation and the production of cytokines following the restimulation of CAR T cells with SKBR3-GFP cells. A total of 50,000 CAR T cells were cocultured with 100,000 target cells for 5 hours in the presence of CD107a antibody (table S3) and 1x Brefeldin A (BioLegend). Following coculture, cells were stained for dead cells (Zombie NIR; BioLegend) and surface markers (CD4 and CD8; table S3), fixed using Fixation Buffer (BioLegend), and stained for the intracellular accumulation of IFN-γ and TNFα (table S3) in 1x Permeabilization Buffer (BioLegend). Samples were analyzed using a Fortessa LSR flow cytometer (BD) or sorted using a FACSAria Fusion (BD).

Calculations of enrichment scores following FACS-based selection

After 9 days of RAS, cells were restimulated for 5 hours with SKBR3 tumor cells and stained for degranulation and cytokine production, as described above. Cells were then sorted using a FACSAria Fusion (BD). As a baseline, CD4- or CD8-positive library CAR T cells were sorted. Next, for each CD4 or CD8 T cell subset, CD107a or IFN-γ positive cell fractions were sorted separately. All sorted cell fractions contained between 5000 and 50,000 cells. Following deep sequencing,

relative library frequencies were calculated. For each independent enrichment sort sample, $\log_2$ fold changes were calculated as the ratio of post-sort frequencies to pre-sort frequencies on day 9. These $\log_2$ fold changes were then used to compute *z* scores.

Single-cell RNA sequencing

Library CAR T cells derived from two healthy donors were subjected to a RAS assay, as previously described. At days 0, 6, and 12 of the RAS assay, CAR library T cells were cocultured with SKBR3-GFP cells for 6 hours in IL-2 (30 IU/ml). Following this time, the cocultures were washed with FACS buffer and stained using DRAQ7, and the live GFP-negative population was sorted using a FACSAria Fusion (BD). Cells were then stained using 20 Totalseq B antibodies (table S4) and introduced into the Chromium Single Cell 3′ scRNAseq pipeline v3.1 (10X Genomics) following the manufacturer's guidelines (User guide CG000317 Rev D). In short, 20,000 cells were loaded into each Chromium chip lane to generate single-cell emulsions containing barcoded oligonucleotides that allow the generation of barcoded cDNA from mRNA and oligo-tagged antibodies. Using the amplified cDNA as a template, scRNAseq and scCITEseq libraries were generated and sequenced using the Illumina NovaSeq platform.

Single-cell CAR sequencing

The demultiplexing of the CAR library to define the CAR identity for each cell in scRNAseq data was achieved using an adapted version of a previously described scCARseq methodology (fig. S3) (*16*). Using 10 μl of the cDNA product resulting from the single-cell sequencing pipeline, the 3′UTR region of the CAR transcripts, containing a CAR variant-specific barcode (CAR-BC), was amplified using F3 and R3 primers (table S2) and KAPA-Hifi polymerase (Roche). Following a 1X SPRIselect bead DNA cleanup (Beckman Coulter), the DNA product containing partial Illumina-specific adaptors was further amplified and indexed using the Dual Index Kit TT, Set A primers (10X Genomics, PN-1000215). The final scCARseq library was then purified using a 1X-0.6X double-sided SPRIselect bead DNA cleanup (Beckman Coulter) and sequenced with the Illumina platform using the same cycle scheme as the scRNAseq and scCITEseq libraries. scCARseq data analysis was conducted using the Biostrings package in R. Only cells with at least two different unique molecular identifiers (UMIs) defining the same CAR annotation were accepted.

Single-cell sequencing data analysis

The raw sequencing data were aligned to the GRCh38 human reference genome using Cell Ranger (10X Genomics, version 6.0.0) and imported into R (version 4.2.3) to perform downstream analysis using the Seurat package (version 4.3.0.1). In the first place, only cells assigned to a single CAR variant were selected. Low-quality cells were removed on the basis of the detection of a low number of genes (nFeature_RNA > 300), high number of gene expression UMIs (nFeature_RNA < 50,000), high number of antibody-derived tags (ADTs) UMIs (nCount_ADT < 30,000), or a high percentage of mitochondrial genes (percent.mt < 20). Last, to correct for clonal expansion that may occur through RAS, a subsampling step was performed; for each sample (different time point or donor), CAR variants exceeding two times the theoretical balanced library distribution (maximum 6.25% of cells per CAR variant) were randomly subsampled to meet this criteria.

The resulting 58,949 single-cell transcriptomes were then normalized, scaled while regressing out the effect of cell cycle phase and percent of mitochondrial genes, and lastly integrated using Harmony (*43*) (applying a lambda of 1 and 200 for sample variables "Donor" and "Time," respectively). Dimensionality reduction using UMAP and unsupervised cell clustering was then used to visualize and analyze the resulting T cell phenotypes. ADT data was normalized using dsb (*44*) in Python using the parameters "pseudocount = 10" and "denoise counts = True." Empty droplets were estimated by dsb from the raw output of Cell Ranger after the exclusion of the cell-containing barcodes found in the filtered output. RNA and ADT data were combined in the annotation of cells as CD4 or CD8. The Seurat object was then further split by CD4/CD8 subsets and time point to perform a more resolved transcriptomic analysis. This analysis included the use of a single-cell gene set scoring function from the Seurat package (AddModuleScore) using the gene sets in table S5 and pseudotime and trajectory analysis using the Monocle3 (*45*) and Slingshot (*46*) packages.

RNAvelocity analysis

VeloCyto package (version 0.17.17) was used to estimate the spliced and unspliced single cell counts using the "velocyto run10x" command with a repeat annotation from UCSC genome browser repeatmasker (*47*) using the GRCh38-2020-A genome. scVelo (version 0.3.2) was then used to calculate the velocity vectors using the dynamic estimation method, which were visualized on a UMAP representation. We ran scVelo and the UMAP on the CD4 and CD8 subsets separately.

Annotation transfer analysis

The scRNAseq count data from Bai *et al.* (*31*), accessible under the Gene Expression Omnibus (GEO) database accession number GSE197215, was downloaded, imported into R (version 4.2.3), and converted into a Seurat object using the Seurat package (version 4.3.0.1). A total of 61,589 cells were used (30,484 CD19-3 T3 stimulated and 31,105 unstimulated cells). The data were normalized, scaled, and integrated using Harmony (*43*). The annotation transfer was then performed using the FindTransferAnchors() and TransferData() functions from the Seurat package. The clinical response data were extracted from the original manuscript.

Supplementary Materials

This PDF file includes:

Figs. S1 to S13
Tables S1 to S5

REFERENCES AND NOTES

1. J. J. Melenhorst, G. M. Chen, M. Wang, D. L. Porter, C. Chen, M. A. Collins, P. Gao, S. Bandyopadhyay, H. Sun, Z. Zhao, S. Lundh, I. Pruteanu-Malinici, C. L. Nobles, S. Maji, N. V. Frey, S. I. Gill, A. W. Loren, L. Tian, I. Kulikovskaya, M. Gupta, D. E. Ambrose, M. M. Davis, J. A. Fraietta, J. L. Brogdon, R. M. Young, A. Chew, B. L. Levine, D. L. Siegel, C. Alanio, E. J. Wherry, F. D. Bushman, S. F. Lacey, K. Tan, C. H. June, Decade-long leukaemia remissions with persistence of $CD4^+$ CAR T cells. *Nature* **602**, 503–509 (2022).
2. K. M. Cappell, J. N. Kochenderfer, Long-term outcomes following CAR T cell therapy: What we know so far. *Nat. Rev. Clin. Oncol.* **20**, 359–371 (2023).
3. V. Wang, M. Gauthier, V. Decot, L. Reppel, D. Bensoussan, Systematic review on CAR-T cell clinical trials up to 2022: Academic center input. *Cancers* **15**, 1003 (2023).
4. N. N. Shah, T. J. Fry, Mechanisms of resistance to CAR T cell therapy. *Nat. Rev. Clin. Oncol.* **16**, 372–385 (2019).
5. N. Singh, M. V. Maus, Synthetic manipulation of the cancer-immunity cycle: CAR-T cell therapy. *Immunity* **56**, 2296–2310 (2023).

6. J. Julamanee, S. Terakura, K. Umemura, Y. Adachi, K. Miyao, S. Okuno, E. Takagi, T. Sakai, D. Koyama, T. Goto, R. Hanajiri, M. Hudecek, P. Steinberger, J. Leitner, T. Nishida, M. Murata, H. Kiyoi, Composite CD79A/CD40 co-stimulatory endodomain enhances CD19CAR-T cell proliferation and survival. *Mol. Ther.* **29**, 2677–2690 (2021).
7. X. Zhou, H. Cao, S.-Y. Fang, R. D. Chow, K. Tang, M. Majety, M. Bai, M. B. Dong, P. A. Renauer, X. Shang, K. Suzuki, A. Levchenko, S. Chen, CTLA-4 tail fusion enhances CAR-T antitumor immunity. *Nat. Immunol.* **24**, 1499–1510 (2023).
8. H. Kintz, E. Nylen, A. Barber, Inclusion of Dap10 or 4-1BB costimulation domains in the chPD1 receptor enhances anti-tumor efficacy of T cells in murine models of lymphoma and melanoma. *Cell. Immunol.* **351**, 104069 (2020).
9. R. M.-H. Velasco Cárdenas, S. M. Brandl, A. V. Meléndez, A. E. Schlaak, A. Buschky, T. Peters, F. Beier, B. Serrels, S. Taromi, K. Raute, S. Hauri, M. Gstaiger, S. Lassmann, J. B. Huppa, M. Boerries, G. Andrieux, B. Bengsch, W. W. Schamel, S. Minguet, Harnessing CD3 diversity to optimize CAR T cells. *Nat. Immunol.* **24**, 2135–2149 (2023).
10. A. M. Tousley, M. C. Rotiroti, L. Labanieh, L. W. Rysavy, W.-J. Kim, C. Lareau, E. Sotillo, E. W. Weber, S. P. Rietberg, G. N. Dalton, Y. Yin, D. Klysz, P. Xu, E. L. de la Serna, A. R. Dunn, A. T. Satpathy, C. L. Mackall, R. G. Majzner, Co-opting signalling molecules enables logic-gated control of CAR T cells. *Nature* **615**, 507–516 (2023).
11. S. Guedan, A. Madar, V. Casado-Medrano, C. Shaw, A. Wing, F. Liu, R. M. Young, C. H. June, A. D. Posey Jr., Single residue in CD28-costimulated CAR-T cells limits long-term persistence and antitumor durability. *J. Clin. Invest.* **130**, 3087–3097 (2020).
12. J. Feucht, J. Sun, J. Eyquem, Y.-J. Ho, Z. Zhao, J. Leibold, A. Dobrin, A. Cabriolu, M. Hamieh, M. Sadelain, Calibration of CAR activation potential directs alternative T cell fates and therapeutic potency. *Nat. Med.* **25**, 82–88 (2019).
13. K. S. Gordon, T. Kyung, C. R. Perez, P. V. Holec, A. Ramos, A. Q. Zhang, Y. Agarwal, Y. Liu, C. E. Koch, A. Starchenko, B. A. Joughin, D. A. Lauffenburger, D. J. Irvine, M. T. Hemann, M. E. Birnbaum, Screening for CD19-specific chimaeric antigen receptors with enhanced signalling via a barcoded library of intracellular domains. *Nat. Biomed. Eng.* **6**, 855–866 (2022).
14. D. B. Goodman, C. S. Azimi, K. Kearns, A. Talbot, K. Garakani, J. Garcia, N. Patel, B. Hwang, D. Lee, E. Park, V. S. Vykunta, B. R. Shy, C. J. Ye, J. Eyquem, A. Marson, J. A. Bluestone, K. T. Roybal, Pooled screening of CAR T cells identifies diverse immune signaling domains for next-generation immunotherapies. *Sci. Transl. Med.* **14**, eabm1463 (2022).
15. K. G. Daniels, S. Wang, M. S. Simic, H. K. Bhargava, S. Capponi, Y. Tonai, W. Yu, S. Bianco, W. A. Lim, Decoding CAR T cell phenotype using combinatorial signaling motif libraries and machine learning. *Science* **378**, 1194–1200 (2022).
16. R. Castellanos-Rueda, R. B. Di Roberto, F. Bieberich, F. S. Schlatter, D. Palianina, O. T. P. Nguyen, E. Kapetanovic, H. Läubli, A. Hierlemann, N. Khanna, S. T. Reddy, speedingCARs: Accelerating the engineering of CAR T cells by signaling domain shuffling and single-cell sequencing. *Nat. Commun.* **13**, 6555 (2022).
17. C. M. Bucks, J. A. Norton, A. C. Boesteanu, Y. M. Mueller, P. D. Katsikis, Chronic antigen stimulation alone is sufficient to drive $CD8^+$ T cell exhaustion. *J. Immunol.* **182**, 6697–6708 (2009).
18. J. A. Fraietta, S. F. Lacey, E. J. Orlando, I. Pruteanu-Malinici, M. Gohil, S. Lundh, A. C. Boesteanu, Y. Wang, R. S. O'Connor, W.-T. Hwang, E. Pequignot, D. E. Ambrose, C. Zhang, N. Wilcox, F. Bedoya, C. Dorfmeier, F. Chen, L. Tian, H. Parakandi, M. Gupta, R. M. Young, F. B. Johnson, I. Kulikovskaya, L. Liu, J. Xu, S. H. Kassim, M. M. Davis, B. L. Levine, N. V. Frey, D. L. Siegel, A. C. Huang, E. J. Wherry, H. Bitter, J. L. Brogdon, D. L. Porter, C. H. June, J. J. Melenhorst, Determinants of response and resistance to CD19 chimeric antigen receptor (CAR) T cell therapy of chronic lymphocytic leukemia. *Nat. Med.* **24**, 563–571 (2018).
19. D. Yu, M.-C. Hung, Overexpression of ErbB2 in cancer and ErbB2-targeting strategies. *Oncogene* **19**, 6115–6121 (2000).
20. B. Prinzing, P. Schreiner, M. Bell, Y. Fan, G. Krenciute, S. Gottschalk, MyD88/CD40 signaling retains CAR T cells in a less differentiated state. *JCI Insight* **5**, e136093 (2020).
21. S. Nair, J.-B. Wang, S.-T. Tsao, Y. Liu, W. Zhu, W. B. Slayton, J. S. Moreb, L. Dong, L.-J. Chang, Functional improvement of chimeric antigen receptor through intrinsic interleukin-15Rα signaling. *Curr. Gene Ther.* **19**, 40–53 (2019).
22. J. Eyquem, J. Mansilla-Soto, T. Giavridis, S. J. C. van der Stegen, M. Hamieh, K. M. Cunanan, A. Odak, M. Gönen, M. Sadelain, Targeting a CAR to the *TRAC* locus with CRISPR/Cas9 enhances tumour rejection. *Nature* **543**, 113–117 (2017).
23. V. D. Fedorov, M. Themeli, M. Sadelain, PD-1- and CTLA-4-based inhibitory chimeric antigen receptors (iCARs) divert off-target immunotherapy responses. *Sci. Transl. Med.* **5**, 215ra172 (2013).
24. M. P. Trefny, N. Kirchhammer, P. Auf der Maur, M. Natoli, D. Schmid, M. Germann, L. Fernandez Rodriguez, P. Herzig, J. Lötscher, M. Akrami, J. C. Stinchcombe, M. A. Stanczak, A. Zingg, M. Buchi, J. Roux, R. Marone, L. Don, D. Lardinois, M. Wiese, L. T. Jeker, M. Bentires-Alj, J. Rossy, D. S. Thommen, G. M. Griffiths, H. Läubli, C. Hess, A. Zippelius, Deletion of *SNX9* alleviates CD8 T cell exhaustion for effective cellular cancer immunotherapy. *Nat. Commun.* **14**, 86 (2023).
25. C. R. Good, M. A. Aznar, S. Kuramitsu, P. Samareh, S. Agarwal, G. Donahue, K. Ishiyama, N. Wellhausen, A. K. Rennels, Y. Ma, L. Tian, S. Guedan, K. A. Alexander, Z. Zhang, P. C. Rommel, N. Singh, K. M. Glastad, M. W. Richardson, K. Watanabe, J. L. Tanyi, M. H. O'Hara, M. Ruella, S. F. Lacey, E. K. Moon, S. J. Schuster, S. M. Albelda, L. L. Lanier, R. M. Young, S. L. Berger, C. H. June, An NK-like CAR T cell transition in CAR T cell dysfunction. *Cell* **184**, 6081–6100.E26 (2021).
26. D. Hudrisier, J. Riond, H. Mazarguil, J. E. Gairin, E. Joly, Cutting edge: CTLs rapidly capture membrane fragments from target cells in a TCR signaling-dependent manner. *J. Immunol.* **166**, 3645–3649 (2001).
27. J. Kaminski, R. A. Fleming, F. Alvarez-Calderon, M. B. Winschel, C. McGuckin, E. E. Ho, F. Eng, X. Rui, P. Keskula, L. Cagnin, J. Charles, J. Zavistaski, S. P. Margossian, M. A. Kapadia, J. B. Rottman, J. Lane, S. H. C. Baumeister, V. Tkachev, A. K. Shalek, L. S. Kean, U. Gerdemann, B-cell-directed CAR T-cell therapy activates $CD8^+$ cytotoxic CAR^{neg} bystander T cells in patients and nonhuman primates. *Blood* **144**, 46–60 (2024).
28. A. I. Salter, R. G. Ivey, J. J. Kennedy, V. Voillet, A. Rajan, E. J. Alderman, U. J. Voytovich, C. Lin, D. Sommermeyer, L. Liu, J. R. Whiteaker, R. Gottardo, A. G. Paulovich, S. R. Riddell, Phosphoproteomic analysis of chimeric antigen receptor signaling reveals kinetic and quantitative differences that affect cell function. *Sci. Signal.* **11**, eaat6753 (2018).
29. O. U. Kawalekar, R. S. O'Connor, J. A. Fraietta, L. Guo, S. E. McGettigan, A. D. Posey Jr., P. R. Patel, S. Guedan, J. Scholler, B. Keith, N. W. Snyder, I. A. Blair, M. C. Milone, C. H. June, Distinct signaling of coreceptors regulates specific metabolism pathways and impacts memory development in CAR T Cells. *Immunity* **44**, 380–390 (2016).
30. V. Wittibschlager, U. Bacher, K. Seipel, N. Porret, G. Wiedemann, C. Haslebacher, M. Hoffmann, M. Daskalakis, D. Akhoundova, T. Pabst, CAR T-cell persistence correlates with improved outcome in patients with B-Cell lymphoma. *Int. J. Mol. Sci.* **24**, 5688 (2023).
31. Z. Bai, S. Woodhouse, Z. Zhao, R. Arya, K. Govek, D. Kim, S. Lundh, A. Baysoy, H. Sun, Y. Deng, Y. Xiao, D. M. Barrett, R. M. Myers, S. A. Grupp, C. H. June, R. Fan, P. G. Camara, J. J. Melenhorst, Single-cell antigen-specific landscape of CAR T infusion product identifies determinants of CD19-positive relapse in patients with ALL. *Sci. Adv.* **8**, eabj2820 (2022).
32. R. B. Di Roberto, S. G. Peisajovich, The role of domain shuffling in the evolution of signaling networks. *J. Exp. Zool. B Mol. Dev. Evol.* **322**, 65–72 (2014).
33. L. Labanieh, C. L. Mackall, CAR immune cells: Design principles, resistance and the next generation. *Nature* **614**, 635–648 (2023).
34. S. J. Priceman, E. A. Gerdts, D. Tilakawardane, K. T. Kennewick, J. P. Murad, A. K. Park, B. Jeang, Y. Yamaguchi, X. Yang, R. Urak, L. Weng, W.-C. Chang, S. Wright, S. Pal, R. E. Reiter, A. M. Wu, C. E. Brown, S. J. Forman, Co-stimulatory signaling determines tumor antigen sensitivity and persistence of CAR T cells targeting PSCA+ metastatic prostate cancer. *Oncoimmunology* **7**, e1380764 (2018).
35. W. Khopanlert, P. Choochuen, K. Maneechai, N. Jangphattananont, S. Ung, S. Okuno, P. Steinberger, J. Leitner, S. Sangkhathat, P. Viboonjuntra, S. Terakura, J. Julamanee, Co-stimulation of CD28/CD40 signaling molecule potentiates CAR-T cell efficacy and stemness. *Mol. Ther. Oncol.* **32**, 200837 (2024).
36. K. S. Schluns, T. Stoklasek, L. Lefrançois, The roles of interleukin-15 receptor α: Trans-presentation, receptor component, or both? *Int. J. Biochem. Cell Biol.* **37**, 1567–1571 (2005).
37. S. Guedan, A. D. Posey Jr., C. Shaw, A. Wing, T. Da, P. R. Patel, S. E. McGettigan, V. Casado-Medrano, O. U. Kawalekar, M. Uribe-Herranz, D. Song, J. J. Melenhorst, S. F. Lacey, J. Scholler, B. Keith, R. M. Young, C. H. June, Enhancing CAR T cell persistence through ICOS and 4-1BB costimulation. *JCI Insight* **3**, e96976 (2018).
38. T. Muliaditan, L. Halim, L. M. Whilding, B. Draper, D. Y. Achkova, F. Kausar, M. Glover, N. Bechman, A. Arulappu, J. Sanchez, K. R. Flaherty, J. Obajdin, K. Grigoriadis, P. Antoine, D. Larcombe-Young, C. M. Hull, R. Buus, P. Gordon, A. Grigoriadis, D. M. Davies, A. Schurich, J. Maher, Synergistic T cell signaling by 41BB and CD28 is optimally achieved by membrane proximal positioning within parallel chimeric antigen receptors. *Cell Rep. Med.* **2**, 100457 (2021).
39. W. Si, Y.-Y. Fan, S.-Z. Qiu, X. Li, E.-Y. Wu, J.-Q. Ju, W. Huang, H.-P. Wang, P. Wei, Design of diversified chimeric antigen receptors through rational module recombination. *iScience* **26**, 106529 (2023).
40. R. Castellanos-Rueda, R. B. Di Roberto, F. S. Schlatter, S. T. Reddy, Leveraging single-cell sequencing for chimeric antigen receptor T Cell therapies. *Trends Biotechnol.* **39**, 1308–1320 (2021).
41. N. J. Haradhvala, M. V. Maus, Understanding mechanisms of response to CAR T-cell therapy through single-cell sequencing: Insights and challenges. *Blood Cancer Discov.* **5**, 86–89 (2024).
42. R. B. Di Roberto, B. M. Scott, S. G. Peisajovich, Directed evolution methods to rewire signaling networks. *Methods Mol. Biol.* **1596**, 321–337 (2017).
43. I. Korsunsky, N. Millard, J. Fan, K. Slowikowski, F. Zhang, K. Wei, Y. Baglaenko, M. Brenner, P.-R. Loh, S. Raychaudhuri, Fast, sensitive and accurate integration of single-cell data with Harmony. *Nat. Methods* **16**, 1289–1296 (2019).
44. M. P. Mulè, A. J. Martins, J. S. Tsang, Normalizing and denoising protein expression data from droplet-based single cell profiling. *Nat. Commun.* **13**, 2099 (2022).

45. C. Trapnell, D. Cacchiarelli, J. Grimsby, P. Pokharel, S. Li, M. Morse, N. J. Lennon, K. J. Livak, T. S. Mikkelsen, J. L. Rinn, The dynamics and regulators of cell fate decisions are revealed by pseudotemporal ordering of single cells. *Nat. Biotechnol.* **32**, 381–386 (2014).
46. K. Street, D. Risso, R. B. Fletcher, D. Das, J. Ngai, N. Yosef, E. Purdom, S. Dudoit, Slingshot: Cell lineage and pseudotime inference for single-cell transcriptomics. *BMC Genomics* **19**, 477 (2018).
47. G. La Manno, R. Soldatov, A. Zeisel, E. Braun, H. Hochgerner, V. Petukhov, K. Lidschreiber, M. E. Kastriti, P. Lönnerberg, A. Furlan, J. Fan, L. E. Borm, Z. Liu, D. van Bruggen, J. Guo, X. He, R. Barker, E. Sundström, G. Castelo-Branco, P. Cramer, I. Adameyko, S. Linnarsson, P. V. Kharchenko, RNA velocity of single cells. *Nature* **560**, 494–498 (2018).

Acknowledgments: We thank R. B. Di Roberto, F. Bieberich, F. S. Schlatter, A. Mei, and K. Letscher for valuable scientific discussions. We thank the ETH Zurich D-BSSE Single Cell facility and the ETH Zurich D-BSSE Genomics facility for the excellent support and assistance throughout this study. **Funding:** This work was supported by the NCCR Molecular Systems Engineering, Switzerland (to S.T.R.), the Personalized Health and Related Technologies (to S.T.R.), the IBM Exploratory Challenge (AI-driven engineering of the immune system) (to M.R.M.), the European Union's Horizon 2020 research and innovation programme–Marie Skłodowska-Curie grant agreement no. 955321 (to A.D.), and the ThinkSwiss Research Scholarship (to J.A.F.). **Author contributions:** Conceptualization: R.C.-R. and S.T.R. Methodology: R.C.-R., J.L.F., and S.T.R. Investigation: R.C.-R., K.-L.K.W., J.L.F., and J.A.F. Data analysis: R.C.-R., K.-L.K.W., and A.D. Supervision: R.C.-R., S.T.R., and M.R.M. Resources: S.T.R. and M.R.M. Writing—original draft: R.C.-R. and S.T.R. Writing—review and editing: All the authors. **Competing interests:** S.T.R. holds shares of Alloy Therapeutics, Engimmune Therapeutics and Encelta. S.T.R. is on the scientific advisory board of Alloy Therapeutics, Engimmune Therapeutics, and Encelta. S.T.R. is a member of the board of directors of Engimmune Therapeutics and GlycoEra. All other authors declare that they have no competing interests. **Data and materials availability:** All data needed to evaluate the conclusions in the paper are present in the paper and/or the Supplementary Materials. The raw and processed single-cell sequencing data generated in this study has been deposited in the GEO database under accession number GSE262686.

Submitted 22 March 2024
Accepted 10 January 2025
Published 14 February 2025
10.1126/sciadv.adp4008